Altered gating and regulation of a carboxy-terminal ClC channel mutant expressed in the Caenorhabditis elegans oocyte

Jerod Denton, Keith Nehrke, Xiaoyan Yin, Andrew M. Beld and Kevin Strange

Am J Physiol Cell Physiol 290:1109-1118, 2006. First published Nov 23, 2005;
doi:10.1152/ajpcell.00423.2005

Am J Physiol Cell Physiol 290: C1109–C1118, 2006.
First published November 23, 2005; doi:10.1152/ajpcell.00423.2005.

Altered gating and regulation of a carboxy-terminal ClC channel mutant expressed in the *Caenorhabditis elegans* oocyte

Jerod Denton,[1] Keith Nehrke,[2] Xiaoyan Yin,[1] Andrew M. Beld,[1] and Kevin Strange[1]

[1]*Departments of Anesthesiology, Molecular Physiology and Biophysics, and Pharmacology, Vanderbilt University Medical Center, Nashville, Tennessee; and* [2]*Nephrology Unit, Department of Medicine, University of Rochester Medical Center, Rochester, New York*

Submitted 22 August 2005; accepted in final form 18 November 2005

Denton, Jerod, Keith Nehrke, Xiaoyan Yin, Andrew M. Beld, and Kevin Strange. Altered gating and regulation of a carboxy-terminal ClC channel mutant expressed in the *Caenorhabditis elegans* oocyte. *Am J Physiol Cell Physiol* 290: C1109–C1118, 2006. First published November 23, 2005; doi:10.1152/ajpcell.00423.2005.—CLH-3a and CLH-3b are swelling-activated, alternatively spliced *Caenorhabditis elegans* ClC anion channels that have identical membrane domains but exhibit marked differences in their cytoplasmic NH_2 and COOH termini. The major differences include a 71-amino acid CLH-3a NH_2-terminal extension and a 270-amino acid extension of the CLH-3b COOH terminus. Splice variation gives rise to channels with striking differences in voltage, pH, and Cl^- sensitivity. On the basis of structural and functional insights gained from crystal structures of bacterial ClCs, we suggested previously that these functional differences are due to alternative splicing of the COOH terminus that may change the accessibility and/or function of pore-associated ion-binding sites. We recently identified a mutant worm strain harboring a COOH-terminal deletion mutation in the *clh-3* gene. This mutation removes 101 COOH-terminal amino acids unique to CLH-3b and an additional 64 upstream amino acids shared by both channels. CLH-3b is expressed in the worm oocyte, which allowed us to characterize the mutant channel, CLH-3bΔC, in its native cellular environment. CLH-3bΔC exhibits altered voltage-dependent gating as well as pH and Cl^- sensitivity that resemble those of CLH-3a. This mutation also alters channel inhibition by Zn^{2+}, prevents ATP depletion-induced activation, and dramatically reduces volume sensitivity. These results suggest that the deleted COOH-terminal region of CLH-3bΔC functions to modulate channel sensitivity to voltage and extracellular ions. This region also likely plays a role in channel regulation and cell volume sensitivity. Our findings contribute to a growing body of evidence indicating that cytoplasmic domains play key roles in the gating and regulation of eukaryotic ClCs.

chloride; cell volume; voltage-gated anion channel

MEMBERS OF THE CLC SUPERFAMILY of voltage-gated Cl^- channels are present in all phyla and function in diverse and essential physiological processes (20). Determination of bacterial ClC crystal structures by MacKinnon and co-workers (12, 13) marked a breakthrough in understanding ClC channel gating. ClCs are homodimers, and each monomer is comprised of 18 α-helical domains, 17 of which are intramembrane (12). Monomers form a single, independently gated pore or protopore. Protopore gating is a fast process and is thought to be mediated by the movement of a highly conserved glutamate residue located adjacent to the selectivity filter (13) and perhaps larger-scale structural rearrangements of the pore (1). Many ClC channels also exhibit a slow or common gating process that opens and closes the two protopores simultaneously (Refs. 17, 22; for review, see Ref. 20). The molecular basis of slow gating is unknown but may involve large-scale channel conformational changes (5, 26, 31).

Eukaryotic ClCs have extensive cytoplasmic NH_2 and COOH termini that are absent from crystallized bacterial ClC proteins. In addition, the COOH termini of all eukaryotic ClC channels contain two cystathionine-β-synthase (CBS) domains (3, 20). The bacterial ClC crystal structures indicate that the last α-helix immediately preceding the cytoplasmic COOH terminus contributes directly to the coordination of Cl^- within the channel selectivity filter (12). Dutzler et al. (12) postulated that the interaction of this α-helix with cytoplasmic structures could provide a mechanism for regulating channel-gating properties and activity. Consistent with this idea, mutagenesis studies have demonstrated that cytoplasmic NH_2 and COOH termini play important roles in ClC gating (8, 15, 16, 19, 30). COOH-terminal mutations in ClC-1 and ClC-2 are associated with myotonia and epilepsy (4, 18, 25). Recent studies have suggested that CBS domains may function in slow gating (14). However, despite their obvious importance, the precise structural and functional relationships of cytoplasmic NH_2 and COOH termini are poorly defined.

Six ClC-type anion channel-encoding genes, termed *clh-1–clh-6* or *ceclc-1–ceclc-6*, are present in the *Caenorhabditis elegans* genome (2, 23, 29). The six nematode ClC genes are representative of the three major subfamilies of mammalian ClC genes. Two CLH-3 splice variants, termed CLH-3a and CLH-3b, have been cloned from *C. elegans* (23, 29). These proteins have identical intramembrane domains but differ significantly in their cytoplasmic NH_2 and COOH termini. The major differences include a 71-amino acid NH_2-terminal extension on CLH-3a and a 270-amino acid extension of the CLH-3b COOH terminus. CLH-3b is expressed in the *C. elegans* oocyte and gives rise to a swelling- and meiotic cell cycle-regulated Cl^- current (9).

CLH-3a and CLH-3b exhibit striking differences in voltage sensitivity, activation kinetics, and sensitivity to extracellular pH and Cl^- concentration (9). On the basis of structural and functional insights gained from crystallized bacterial ClC proteins (12, 13), we postulated that alternative splicing of the COOH terminus may account for these differences by altering the accessibility and/or function of pore-associated ion-binding sites (9).

Address for reprint requests and other correspondence: K. Strange, Depts. of Anesthesiology, Molecular Physiology and Biophysics, and Pharmacology, Vanderbilt Univ. Medical Center, T-4202 Medical Center North, Nashville, TN 37232-2520 (e-mail: kevin.strange@vanderbilt.edu).

The costs of publication of this article were defrayed in part by the payment of page charges. The article must therefore be hereby marked "*advertisement*" in accordance with 18 U.S.C. Section 1734 solely to indicate this fact.

We recently identified a worm strain harboring an 841-nt deletion in a region of *clh-3* encoding the predicted cytoplasmic COOH termini of CLH-3a and CLH-3b. The deletion removes 101 amino acids that are unique to CLH-3b and another 64 amino acids shared by both splice variants. Mutant CLH-3b channels are functionally expressed in the *C. elegans* oocyte. To begin defining the role of cytoplasmic domains in regulating CLH-3b gating and activity, we characterized the biophysical properties of the mutant channels in their native cellular environment. We have demonstrated in the present study that the deletion mutation of the COOH terminus disrupts volume- and phosphorylation-dependent channel regulation and dramatically alters voltage sensitivity, sensitivity to extracellular H^+ and Cl^-, and inhibition by Zn^{2+}. These studies provide new insights into the role of the cytoplasmic domains in the regulation of ClC gating and activity and provide the foundation for future site-directed mutagenesis and heterologous expression studies.

MATERIALS AND METHODS

C. elegans culture and strains. Nematodes were cultured at 16°C using standard methods (6). Wild-type worms were of the Bristol N2 strain. *clh-3*(*ok768*) worms were provided by the *C. elegans* Gene Knockout Project at the Oklahoma Medical Research Foundation, which is part of the International *C. elegans* Gene Knockout Consortium (http://www.mutantfactory.ouhsc.edu/).

PCR analysis. clh-3(*ok768*) mutant worms were outcrossed three times, and homozygous animals were identified using PCR analysis of genomic DNA isolated from single worms (24) and the primer set 5′-GTCAATTCGCTCATTCGGTT-3′ and 5′-GGTCAAGAAACG-GAAAACCAA-3′ (Fig. 1*A*). To determine the mutant mRNA sequence, oligo(dT) primed cDNA was prepared from RNA isolated from Bristol N2 and *clh-3*(*ok768*) worms using standard techniques. A partial open reading frame was PCR amplified, cloned, and sequenced using the primer set 5′-CCTGATATTCCCCATACAACGTCC-3′ and 5′-TCAGAATTTTTCGTCATGAAC-3′. These primers annealed in exon 11 and exon 19 immediately before the stop codon (see Fig. 1*B*).

Patch-clamp recording of whole cell Cl^- currents in isolated C. elegans oocytes. Gonads were isolated by placing single nematodes in egg buffer (in mM: 118 NaCl, 48 KCl, 2 $CaCl_2$, 2 $MgCl_2$, and 25 HEPES, pH 7.3; 340 mosM) and cutting them behind the pharyngeal bulb and in front of the spermatheca using a 26-gauge needle. Isolated gonads were transferred to a patch-clamp bath chamber mounted on the stage of an inverted microscope. Late-stage oocytes were released spontaneously from the cut end of the gonad.

Patch-clamp electrodes were pulled from 1.5-mm-outer-diameter silanized borosilicate microhematocrit tubes. Currents were measured using an Axopatch 200B (Axon Instruments, Foster City, CA) patch-clamp amplifier with control bath solution containing (in mM) 116 NMDG-Cl, 2 $CaCl_2$, 2 $MgCl_2$, 25 HEPES, and 71 sucrose (pH 7.3; 340 mosM) and a pipette solution containing (in mM) 116 NMDG-Cl, 2 $MgSO_4$, 20 HEPES, 6 CsOH, 1 EGTA, 48 sucrose, 2 ATP, and 0.5 GTP (pH 7.2; 315 mosM). For low-Cl^- experiments, we used a NaCl-based bath solution that was otherwise identical to the NMDG-Cl^- bath solution. Low-NaCl solutions were prepared by isosmotic substitution of sucrose for NaCl. Oocytes were swollen by exposure to a hypotonic (260 mosM) bath solution that contained no added sucrose. Metabolic inhibitors were dissolved as stock solution in DMSO and then added to pipette or bath solutions at a final DMSO concentration of ≤0.01%.

Electrical connections to the patch-clamp amplifier were made using Ag/AgCl wires and 3 M KCl-agar bridges. Data acquisition and analysis were performed using pCLAMP 8 software (Axon Instruments).

RNA interference. RNA interference (RNAi) was performed as described previously (27). Briefly, a DNA template corresponding to the first 847 bp of the open-reading frame of *clh-3* was obtained by PCR, and sense and antisense RNA were synthesized using T7 polymerase (MEGAscript; Ambion, Austin, TX). Template DNA was digested with DNase I, and RNA was precipitated using 3 M sodium acetate and ethanol. Precipitated RNA was washed with 70% ethanol, air dried, and dissolved in water. RNA size, purity, and integrity were assayed on agarose gels. Double-stranded RNA (dsRNA) was formed by annealing sense and antisense RNA at 65°C for 30 min. Annealed dsRNA was diluted into potassium citrate buffer for injection. Worms were injected in one gonad arm with ~1,000,000 molecules of dsRNA.

Statistical analysis. Data are presented as means ± SE. Statistical significance was determined using Student's two-tailed *t*-test. $P \leq 0.05$ was assumed to indicate statistical significance.

RESULTS

clh-3(ok768) allele is a 165-amino acid deletion in the CLH-3 COOH terminus. PCR analysis of genomic DNA from wild-type and *clh-3*(*ok768*) heterozygous and homozygous worms revealed that the *ok768* allele is an ~800-bp deletion (Fig. 1*A*). DNA sequencing demonstrated that the deletion spanned a region of 841 nt that included part of exon 12 and all of exons 13 and 14, which are present only in CLH-3b (23) (Fig. 1*B*). PCR analysis of the mutant mRNA demonstrated that it coded for a protein where a cryptic site in exon 12 was spliced in frame to exon 15 (Fig. 1*B*). Amplification using primers specific for CLH-3a did not yield a PCR product (data not shown).

The mutant transcript lacked sequence coding for COOH-terminal amino acids V604–E768 of the CLH-3b protein (Fig. 1*C*). We termed the deletion mutant protein CLH-3bΔC. Amino acids R668–E768 are unique to CLH-3b and are encoded by exons 13 and 14. Amino acids V604–S667 comprise a domain that is conserved in both CLH-3a and CLH-3b (Fig. 1*C*). Eleven of the amino acids deleted in this region are present in the first CBS domain.

CLH-3bΔC forms channels with altered voltage sensitivity and activation kinetics. To determine whether CLH-3bΔC channels are functional, we recorded whole cell Cl^- currents in oocytes isolated from wild-type and *clh-3*(*ok768*) worms. As shown previously (9, 27, 28), wild-type meiotic cell cycle-arrested, nonswollen oocytes exhibit a small inwardly rectifying CLH-3b current ($I_{CLH\text{-}3b}$) that is activated by strong hyperpolarization. Figure 2*A* shows mean whole cell current traces

Fig. 1. Molecular characteristics of the *clh-3*(*ok768*) allele. *A*: PCR detection of *clh-3* genomic DNA in single wild-type (+/+), *clh-3*(*ok768*)-heterozygous (+/−), and *clh-3*(*ok768*)-homozygous (−/−) worms. *B*: intron-exon structures of wild-type CLH-3a and CLH-3b as well as the CLH-3b deletion mutant CLH-3bΔC. Exons are indicated by solid boxes or arrows. The last exon in each protein is represented by an arrow to indicate the presence of stop codons followed by 3′-UTR. The sequence surrounding the cryptic splice site in the *clh-3*(*ok768*) deletion mutant is exon 12-CTTGTCGGTTCG/CGTACTGAAT-exon 15, where the cryptic splice site is indicated by a slash. *C*: ClustalW alignment of the amino acid sequences of CLH-3a, CLH-3b, and CLH-3bΔC. Regions of identity are shown on black background, except for cystathionine-β-synthase (CBS) domains, which are shown on gray background.

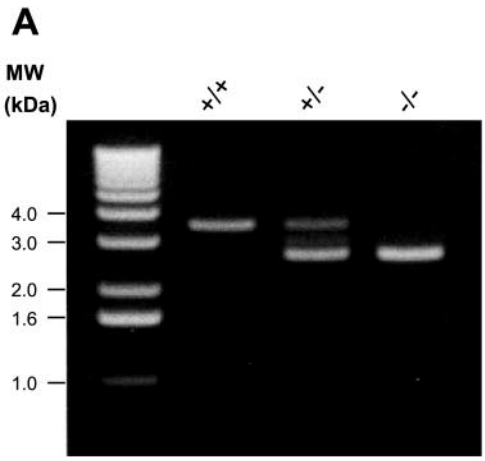

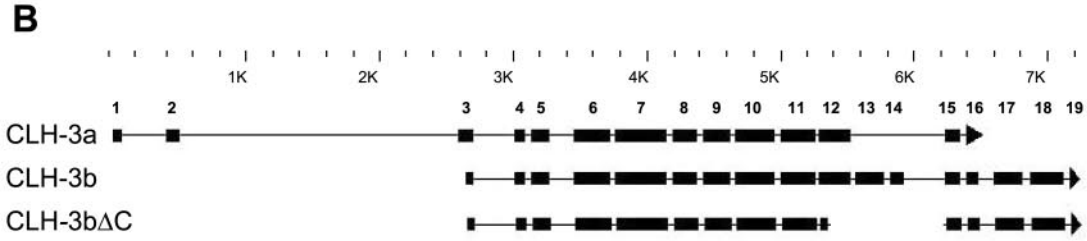

C

```
CLH-3a      1 MPSRTPLSKIEWOSLLPLPPEKSEKDATIENNEELEKIRMPAGKEYDLOPGSHLGVYKTVRGLPIDEDSKSMGIGTKILSKIEKNKTSDGLTIPLTPTTOKOSSSWCSFE
CLH-3b      1 ..........................................................................MGIGTKILSKIEKNKTSDGLTIPLTPTTOKOSSSWCSFE
CLH-3bΔC    1 ..........................................................................MGIGTKILSKIEKNKTSDGLTIPLTPTTOKOSSSWCSFE

CLH-3a    111 SIKTFFRTVIRDWIFLALLGFIMASLSFGMDYAILNLONGOMRLFDLVKEYHFTLAYLVWVGYVVGLILLSAVCAHYIAPOAIGSGIPEMKTILRGVILKEYLSVRTLLS
CLH-3b     40 SIKTFFRTVIRDWIFLALLGFIMASLSFGMDYAILNLONGOMRLFDLVKEYHFTLAYLVWVGYVVGLILLSAVCAHYIAPOAIGSGIPEMKTILRGVILKEYLSVRTLLS
CLH-3bΔC   40 SIKTFFRTVIRDWIFLALLGFIMASLSFGMDYAILNLONGOMRLFDLVKEYHFTLAYLVWVGYVVGLILLSAVCAHYIAPOAIGSGIPEMKTILRGVILKEYLSVRTLLS

CLH-3a    221 KMIGLTLSLGSGLPMGKEGPFVHVASVVASOLTRLVHGSSGGIFENESRSGEMLAAGCAVGVACTFSAPIGGVLFSIEVTSVYFAVRNYWRGFFAATCSATLFRILRMFS
CLH-3b    150 KMIGLTLSLGSGLPMGKEGPFVHVASVVASOLTRLVHGSSGGIFENESRSGEMLAAGCAVGVACTFSAPIGGVLFSIEVTSVYFAVRNYWRGFFAATCSATLFRILRMFS
CLH-3bΔC  150 KMIGLTLSLGSGLPMGKEGPFVHVASVVASOLTRLVHGSSGGIFENESRSGEMLAAGCAVGVACTFSAPIGGVLFSIEVTSVYFAVRNYWRGFFAATCSATLFRILRMFS

CLH-3a    331 VSAAVTVEAHYOTNFPPONVFLPOELPIFALIGLVCGLAGSIFVYLHRRTVLFLRRNWLAKMIFOKYWLIYPIFIATFISSLSFPLGLGKFMGGEERFSHTMKEFFVDCA
CLH-3b    260 VSAAVTVEAHYOTNFPPONVFLPOELPIFALIGLVCGLAGSIFVYLHRRTVLFLRRNWLAKMIFOKYWLIYPIFIATFISSLSFPLGLGKFMGGEERFSHTMKEFFVDCA
CLH-3bΔC  260 VSAAVTVEAHYOTNFPPONVFLPOELPIFALIGLVCGLAGSIFVYLHRRTVLFLRRNWLAKMIFOKYWLIYPIFIATFISSLSFPLGLGKFMGGEERFSHTMKEFFVDCA

CLH-3a    441 WTAPPNDSYACPMPTSNATSSDSFDIRHWKGDNYDYSPFVTLSSFOVVYFFLAILASTLPVPSGIFMPVFVLGAAFGRLVGEGVFSLDPYGHISGDIOFFVRPGVYAVVG
CLH-3b    370 WTAPPNDSYACPMPTSNATSSDSFDIRHWKGDNYDYSPFVTLSSFOVVYFFLAILASTLPVPSGIFMPVFVLGAAFGRLVGEGVFSLDPYGHISGDIOFFVRPGVYAVVG
CLH-3bΔC  370 WTAPPNDSYACPMPTSNATSSDSFDIRHWKGDNYDYSPFVTLSSFOVVYFFLAILASTLPVPSGIFMPVFVLGAAFGRLVGEGVFSLDPYGHISGDIOFFVRPGVYAVVG

CLH-3a    551 AAAFCGAVTHTVSVAVIVFELTGOLCHLLPVMIAVLIANAVASYLOPSIYDSIIRIKNLPYLPDIPHTTSLYHOMLIEOFMISPLVYIAKDSTVGDIKRALETKTRIRAF
CLH-3b    480 AAAFCGAVTHTVSVAVIVFELTGOLCHLLPVMIAVLIANAVASYLOPSIYDSIIRIKNLPYLPDIPHTTSLYHOMLIEOFMISPLVYIAKDSTVGDIKRALETKTRIRAF
CLH-3bΔC  480 AAAFCGAVTHTVSVAVIVFELTGOLCHLLPVMIAVLIANAVASYLOPSIYDSIIRIKNLPYLPDIPHTTSLYHOMLIEOFMISPLVYIAKDSTVGDIKRALETKTRIRAF

CLH-3a    661 PLVENMESLALVGSVSRSQLQRYVDSQIGTKARFAEATRRIKORLEDEESERKRREESKSDDTEDSLETTGAGERRAS.....................................
CLH-3b    590 PLVENMESLALVGSVSRSOLORYVDSQIGTKARFAEATRRIKORLEDEESERKRREESKSDDTEDSLETTGAGERRASRFLIVPVAKNGPOVAKNETLTGLSEENARKIL
CLH-3bΔC  590 PLVENMESLALVGS..........................................................................................................

CLH-3a    739 ..................................................................RTEWEDMMLNOKLDLSQLDIDSTPFQLSEYTSLFKAHSLFS
CLH-3b    700 TVEEKOALFDAASLATPKREMSGKTINPVHIESHHTIGDIFRSITHLSFGRONFPKKNNHNEFDLFGEBRTEWEDMMLNOKLDLSQLDIDSTPFOLSEYTSLFKAHSLFS
CLH-3bΔC  603 ..................................................................RTEWEDMMLNOKLDLSQLDIDSTPFQLSEYTSLFKAHSLFS

CLH-3a    787 LLGLNRAYVTKKGQLIGVVALKEVCFLISRKK*.....................................................................................
CLH-3b    810 LLGLNRAYVTKKGQLIGVVALKELRLAIEYLOSGKVPTPGMSIFNEPPTEOSIYEKSARLESGRATGDAONAAFVTDNGEDDAONDYIOPPLEVVRRGALTPNRMSELTR
CLH-3bΔC  645 LLGLNRAYVTKKGQLIGVVALKELRLAIEYLOSGKVPTPGMSIFNEPPTEOSIYEKSARLESGRATGDAONAAFVTDNGEDDAONDYIOPPLEVVRRGALTPNRMSELTR

CLH-3a    819 .....................................................................................................
CLH-3b    920 LENVRTTPESPHFEVSSPSTSSSCVSIDFSPLDAANSENGSVGGLVLNVPSLPTRARSANELTRONTHVOINLPDDVHDEKF*
CLH-3bΔC  755 LENVRTTPESPHFEVSSPSTSSSCVSIDESPLDAANSENGSVGGLVLNVPSLPTRARSANELTRONTHVOINLPDDVHDEKF*
```

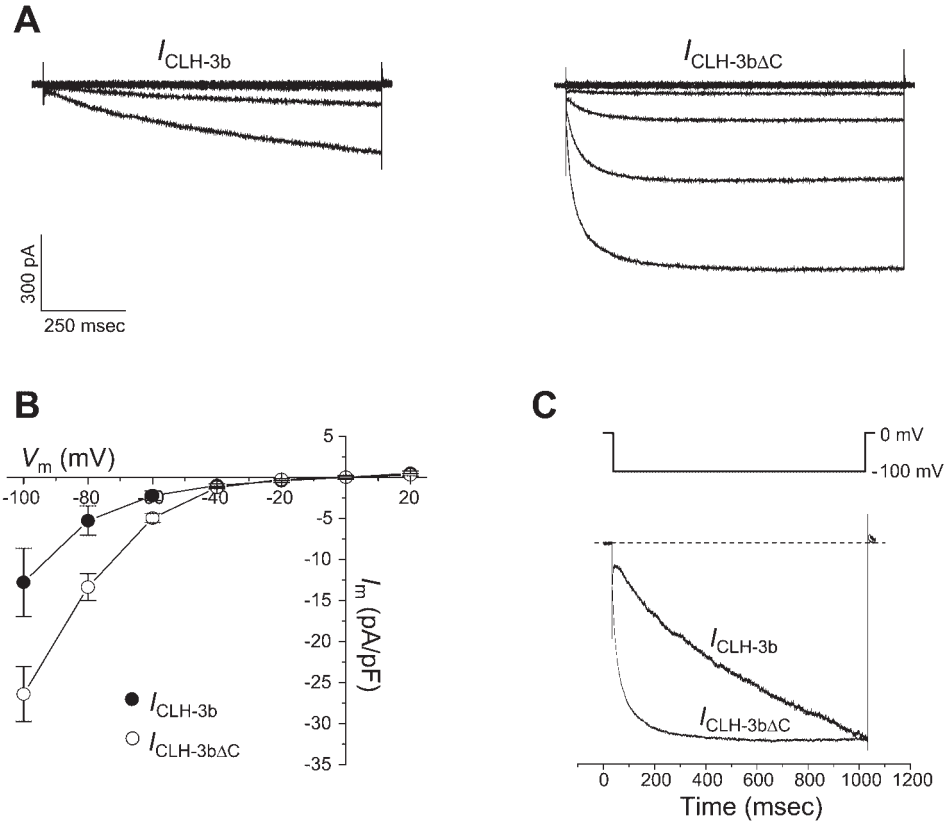

Fig. 2. Cl^- currents recorded from nonswollen, meiotic cell cycle-arrested wild-type and *clh-3*(*ok768*) oocytes. *A*: mean whole cell CLH-3b (n = 9) and CLH-3bΔC (n = 18) currents. Currents were evoked by voltage clamping oocytes between −100 and +20 mV for 1 s in 20-mV increments from a holding potential of 0 mV. Each test pulse was followed by a 1-s recovery period at 0 mV. *B*: current-voltage (*I-V*) relationships for inwardly rectifying CLH-3b current (I_{CLH-3b}) and mean steady-state CLHb-3ΔC current ($I_{CLH-3b\Delta C}$). Values are means ± SE (n = 9–18) of current values measured during the last 20 ms of each test pulse. *C*: comparison of I_{CLH-3b} and $I_{CLH-3b\Delta C}$ activation kinetics at −100 mV. The $I_{CLH-3b\Delta C}$ trace has been scaled by a factor of 2.1 and superimposed over the I_{CLH-3b} trace for comparison. The zero-current level is indicated by a dashed line.

recorded in nine wild-type oocytes. The mean amplitude of this current recorded during the last 20 ms of the 1-s test pulse to −100 mV was −13 pA/pF (Fig. 2*B*).

Nonswollen, cell cycle-arrested oocytes from *clh-3*(*ok768*) worms also exhibited inwardly rectifying Cl^- currents. Figure 2*A* shows mean whole cell current traces recorded from 18 *clh-3*(*ok768*) oocytes. The mean steady-state CLHb-3ΔC current ($I_{CLH-3b\Delta C}$) amplitude measured during the last 20 ms of the −100-mV test pulse was −26 pA/pF (Fig. 2*B*), which was significantly ($P < 0.02$) greater than that observed in wild-type worms.

To test whether this current was due to the activity of a *clh-3*-encoded channel, we performed RNAi experiments. *clh-3* RNAi disrupts CLH-3 channel expression in the *C. elegans* oocyte (9, 27, 28). Steady-state current amplitude recorded at −100 mV in oocytes isolated from *clh-3*(*ok768*) worms injected with *clh-3* dsRNA was inhibited >95% ($P <$ 0.01) to a mean ± SE value of −1.2 ± 0.8 pA/pF (n = 3). These results demonstrate that whole oocyte Cl^- currents in *clh-3*(*ok768*) worms are carried by CLH-3bΔC channels.

The kinetics of hyperpolarization-induced activation of $I_{CLH-3b\Delta C}$ were considerably more rapid than those of I_{CLH-3b}. Figure 2*C* shows average current traces recorded at −100 mV from wild-type and *clh-3*(*ok768*) oocytes. The I_{CLH-3b} trace is scaled by a factor of 2.1 and superimposed over the $I_{CLH-3b\Delta C}$ trace to facilitate comparison of their activation kinetics. In nonswollen, cell cycle-arrested oocytes, I_{CLH-3b} activation can be described by a monoexponential function. The mean ± SE time constant for I_{CLH-3b} activation at −100 mV was 942 ± 190 ms (n = 9). By contrast, $I_{CLH-3b\Delta C}$ activation was a

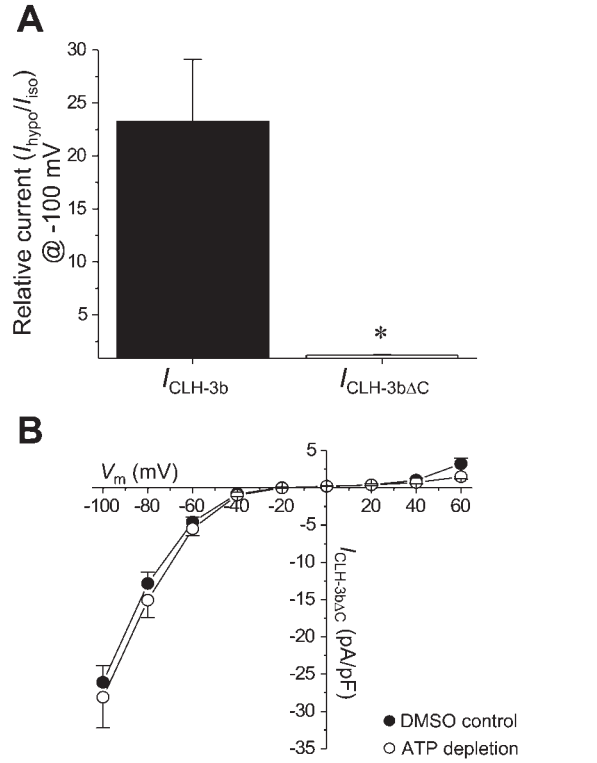

Fig. 3. Regulation of $I_{CLH-3b\Delta C}$ by oocyte swelling and ATP depletion. *A*: relative amplitude (I_{hypo}/I_{iso}) of I_{CLH-3b} and $I_{CLH-3b\Delta C}$ recorded during the last 20 ms of a −100-mV test pulse after hypotonic oocyte swelling for 10 min. Values are means ± SE (n = 6–9). *$P < 0.01$ vs. I_{CLH-3b}. *B*: *I-V* relationships for $I_{CLH-3b\Delta C}$ recorded from metabolically poisoned oocytes or DMSO controls. Values are means ± SE (n = 8).

biexponential process described by fast and slow time constants at −100 mV of ~13 ms and ~58 ms, respectively (discussed in detail below).

As shown previously (27, 28), oocyte swelling dramatically increases $I_{CLH\text{-}3b}$ amplitude. Figure 3*A* shows that hypotonicity induced oocyte swelling for 10-min-activated $I_{CLH\text{-}3b}$ ~23-fold. In marked contrast, $I_{CLH\text{-}3b\Delta C}$ amplitude increased only 1.2-fold in response to oocyte swelling for 10 min (Fig. 3*A*).

ATP depletion activates CLH-3b by inducing net protein dephosphorylation (28). We depleted *clh-3*(*ok768*) oocytes of ATP by exposing them to 5 mM 2-deoxyglucose (2-DG) and 1 μM rotenone in bath solution. After being incubated for 20–30 min, oocytes were patch clamped using an ATP-free pipette solution containing (in μM) 40 oligomycin, 20 rotenone, and 5 iodoacetate. As shown in Fig. 3*B*, ATP depletion had no significant ($P > 0.4$) effect on $I_{CLH\text{-}3b\Delta C}$ amplitude.

Oocyte shrinkage inhibits $I_{CLH\text{-}3b}$ that has been activated by either oocyte swelling or meiotic cell cycle progression (27). However, $I_{CLH\text{-}3b\Delta C}$ amplitude was not significantly ($P > 0.8$) altered by cell shrinkage. Mean ± SE relative current amplitude measured at −100 mV after 10-min exposure of *clh-3*(*ok768*) oocytes to hypertonic saline was 0.98 ± 0.08 ($n = 6$). We conclude that the COOH-terminal deletion mutation drastically reduces CLH-3b volume sensitivity, prevents dephosphorylation-induced channel activation, and alters the kinetic properties of the channel.

Oocyte swelling alters the voltage sensitivity and kinetics of hyperpolarization-induced activation of $I_{CLH\text{-}3b}$ (9, 27). Figure 4*A* shows mean whole cell currents recorded in wild-type and *clh-3*(*ok768*) oocytes swollen for 10 min. Mean CLH-3b and CLH-3bΔC current densities at −100 mV were −175 pA/pF and −25 pA/pF, respectively.

The apparent voltage sensitivities of $I_{CLH\text{-}3b}$ and $I_{CLH\text{-}3b\Delta C}$ recorded in swollen oocytes were considerably different. Figure 4*B* shows Boltzmann relationships for $I_{CLH\text{-}3b}$ and $I_{CLH\text{-}3b\Delta C}$. As described previously by us (9) and by Schriever et al. (29), CLH-3 channels close too rapidly at depolarized potentials for tail currents to be measured reliably. Furthermore, the depolarization-induced potentiation of $I_{CLH\text{-}3b\Delta C}$ (see below) prevented tail current analysis using a negative test pulse. Consequently, we were unable to estimate the voltage dependence of CLH-3bΔC open probability using tail current analysis. We therefore normalized steady-state current values recorded at each test potential to those measured at −100 mV and fitted this relationship using a Boltzmann function. As shown in Fig. 4*B*, $I_{CLH\text{-}3b}$ was activated at more depolarized

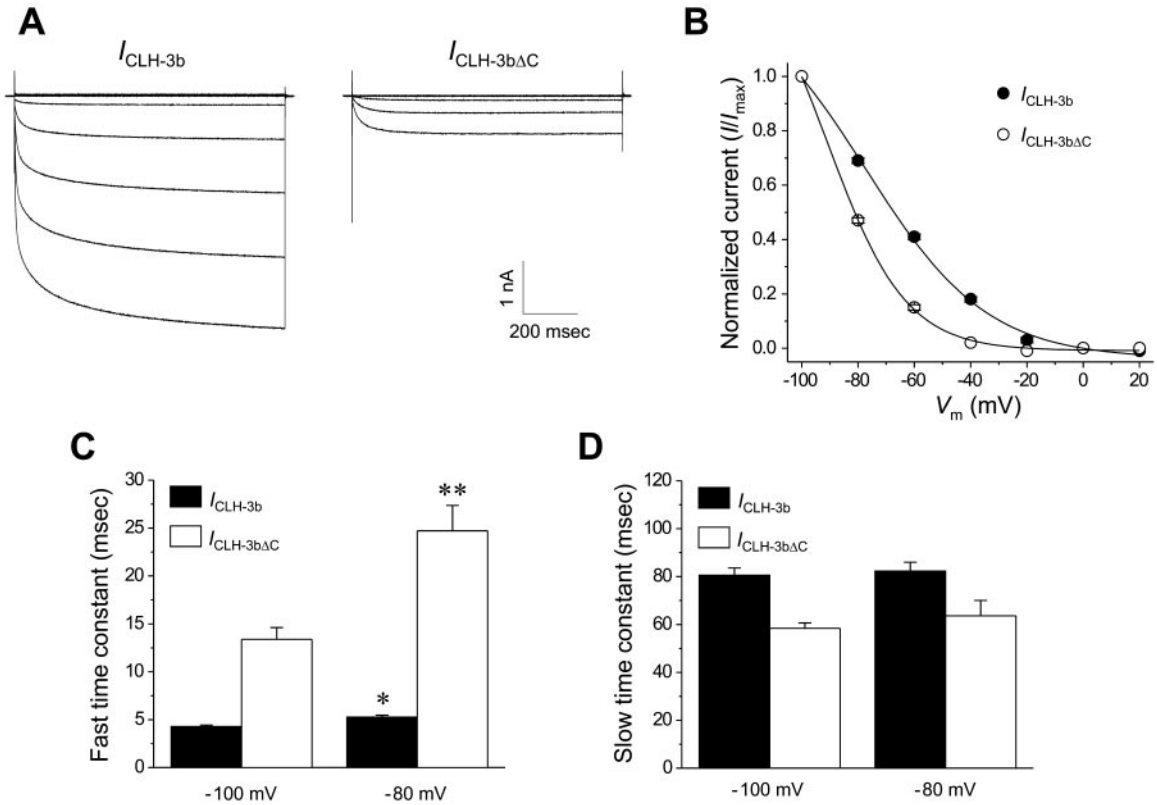

Fig. 4. Voltage- and time-dependent properties of $I_{CLH\text{-}3b}$ and $I_{CLH\text{-}3b\Delta C}$. *A*: mean whole cell $I_{CLH\text{-}3b}$ ($n = 9$) and $I_{CLH\text{-}3b\Delta C}$ ($n = 6$) recorded in worm oocytes swollen for 10 min by exposure to hypotonic bath solution. Voltage-clamp protocol is the same as that described in Fig. 2. *B*: Boltzmann fits of normalized *I-V* relationships for $I_{CLH\text{-}3b}$ and $I_{CLH\text{-}3b\Delta C}$. Steady-state current amplitude recorded at each test potential was normalized to that measured at −100 mV. Fits were performed using the equation

$$I(V_m) = \frac{A_1 - A_2}{1 + e^{(V_m - V_{0.5})/k}} + A_2,$$

in which $V_{0.5}$ is the half-activation potential and k is the slope factor. Values are means ± SE ($n = 6$–9). *C*: comparison of fast-activation time constants for $I_{CLH\text{-}3b}$ and $I_{CLH\text{-}3b\Delta C}$ at −100 mV and −80 mV. *$P < 0.0007$ and **$P < 0.0006$ compared with values measured at −100 mV. Statistical analyses were performed with paired data. *D*: slow-activation time constants for $I_{CLH\text{-}3b}$ and $I_{CLH\text{-}3b\Delta C}$ at −100 and −80 mV. Values in *C* and *D* are means ± SE ($n = 6$–9). Time constants were derived from biexponential fits of the first 200 ms of hyperpolarization-induced current activation.

potentials than $I_{CLH\text{-}3b\Delta C}$, causing a rightward shift in its current-voltage (*I-V*) relationship. The mean ± SE half-activation voltages ($V_{0.5}$) and slope factors (k) derived from the Boltzmann curves for $I_{CLH\text{-}3b}$ and $I_{CLH\text{-}3b\Delta C}$ were −67 ± 0.7 mV and 17 ± 0.6 mV^{-1} ($n = 9$) and −80 ± 0.4 mV ($n = 6$) and 9 ± 0.4 mV^{-1} ($n = 6$), respectively. Similar $V_{0.5}$ and k values for $I_{CLH\text{-}3b\Delta C}$ were observed in nonswollen oocytes (data not shown).

The kinetics of channel activation were estimated by fitting two-term exponential functions that described τ_{fast} and τ_{slow} components of the activation portion of current traces. Because of the small current amplitude of $I_{CLH\text{-}3b\Delta C}$ at −60 mV, reasonable exponential fits could be performed only at −80 mV and −100 mV. The τ_{fast} values for both currents were voltage dependent and increased significantly ($P < 0.0007$) with depolarization (Fig. 4*C*). In contrast, τ_{slow} values for $I_{CLH\text{-}3b}$ and $I_{CLH\text{-}3b\Delta C}$ were voltage independent ($P > 0.2$) over the voltage range tested (Fig. 4*D*).

We also observed statistically significant ($P < 0.0001$) differences in τ_{fast} and τ_{slow} values of $I_{CLH\text{-}3b}$ compared with $I_{CLH\text{-}3b\Delta C}$. However, because the amplitude of $I_{CLH\text{-}3b}$ is much greater than that of $I_{CLH\text{-}3b\Delta C}$ (Fig. 4*A*), the relevance of such apparent differences is unclear at present.

CLH-3bΔC exhibits predepolarization-induced potentiation. The slower activation kinetics and hyperpolarizing shift in the *I-V* relationship of $I_{CLH\text{-}3b\Delta C}$ are reminiscent of the biophysical characteristics of heterologously expressed CLH-3a (9). A striking characteristic of CLH-3a is its sensitivity to conditioning predepolarization. Both we (9) and Schriever et al. (29) showed previously that hyperpolarization-induced activation of CLH-3a is potentiated by prior membrane depolarization. However, native CLH-3b in the nematode oocyte as well as heterologously expressed CLH-3b are virtually insensitive to depolarizing prepulses (9). Given the similarities of voltage-dependent activation of CLH-3bΔC and CLH-3a, we tested the effect of conditioning predepolarization on $I_{CLH\text{-}3b\Delta C}$. Oocytes isolated from *clh-3*(*ok768*) worms were clamped for 3 s at conditioning potentials between −20 mV and +60 mV in 20-mV increments and then stepped to −100 mV for 2 s to activate $I_{CLH\text{-}3b\Delta C}$. Figure 5*A* shows that hyperpolarization-induced activation of $I_{CLH\text{-}3b\Delta C}$ was potentiated by conditioning predepolarization. For example, $I_{CLH\text{-}3b\Delta C}$ amplitude recorded at −100 mV after a conditioning potential of 60 mV was ~1.5-fold that after a conditioning potential of −20 mV (Fig. 5*B*).

Conditioning predepolarization also induces a slow inactivation process at hyperpolarizing test voltages in CLH-3a but not in CLH-3b (9). The current traces shown in Fig. 5*A* demonstrate that depolarizing prepulses induced a similar inactivation process in CLH-3bΔC. Figure 5*C* summarizes the voltage dependence of inactivation of $I_{CLH\text{-}3b\Delta C}$. The degree of inactivation was calculated by normalizing the pseudo-steady-state current (I_{ss}) amplitude recorded during the last 20 ms of the −100-mV test pulse to the peak current (I_{peak}) amplitude recorded between 170 and 270 ms. This time domain was chosen because it bracketed the peak $I_{CLH\text{-}3b\Delta C}$ amplitude after depolarized conditioning pulses (see Fig. 5*A*). $I_{CLH\text{-}3b\Delta C}$ inactivation was rarely observed after a conditioning potential of −20 or 0 mV but became prominent with stronger depolarizing prepulses (Fig. 5*C*). After a conditioning pulse to +60 mV, $I_{CLH\text{-}3b\Delta C}$ was inactivated by ~15% after the current was activated by hyperpolarization to −100 mV.

CLH-3bΔC exhibits altered sensitivity to extracellular Cl^- and pH. Heterologously expressed CLH-3a is significantly more sensitive than CLH-3b to changes in extracellular Cl^- and H^+ concentration (9). We therefore examined the effects

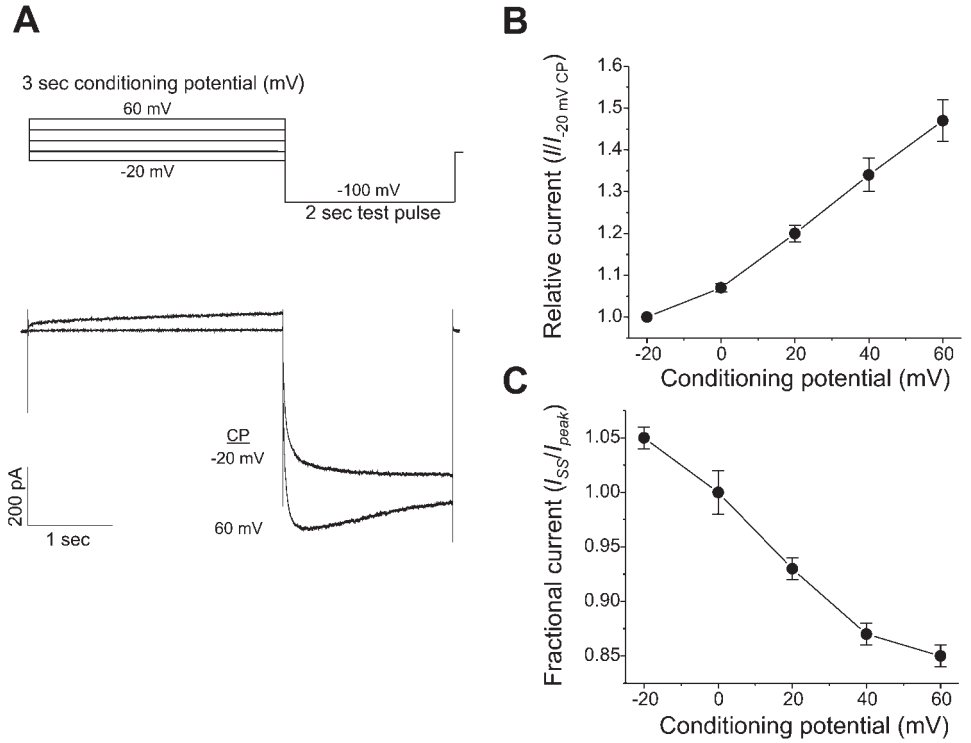

Fig. 5. Depolarization-induced potentiation of $I_{CLH\text{-}3b\Delta C}$ activation. *A*: voltage-clamp protocol and mean $I_{CLH\text{-}3b\Delta C}$ traces ($n = 9$) showing potentiation of $I_{CLH\text{-}3b\Delta C}$ by conditioning predepolarization. Oocytes were voltage clamped for 3 s at condition potentials (CP) between −20 to +60 mV and then stepped to −100 mV for 2 s to activate $I_{CLH\text{-}3b\Delta C}$. For clarity, only current traces evoked after −20-mV and +60-mV CP are shown. *B*: effect of conditioning potential on hyperpolarization-induced activation of $I_{CLH\text{-}3b\Delta C}$. Peak current amplitude was measured between 170 and 270 ms after voltage was stepped to −100 mV. Current values were normalized to that measured after a conditioning pulse of −20 mV (i.e., $I_{-20\ mV}$). Values are means ± SE ($n = 9$). *C*: effect of conditioning potential on inactivation of $I_{CLH\text{-}3b\Delta C}$. Mean normalized pseudo-steady-state current (I_{ss}) was measured during the last 20 ms of the −100-mV test pulse and normalized to peak current (I_{peak}) amplitude. Values are means ± SE ($n = 9$).

of changes in bath Cl^- concentration and pH on $I_{CLH\text{-}3b\Delta C}$. Whole cell currents in *clh-3*(*ok768*) oocytes were recorded in control bath (124 mM Cl^-) and 30 s after switching to a 16 mM Cl^- bath solution. Figure 6*A* shows mean ± SE currents recorded between −100 mV and +40 mV in control and low-Cl^- bath solutions. Reduction of Cl^- inhibited $I_{CLH\text{-}3b\Delta C}$. At −100 mV, for example, $I_{CLH\text{-}3b\Delta C}$ amplitude was reduced ~24% ($P < 0.0001$). A similar change in bath Cl^- concentration has no effect on heterologously expressed $I_{CLH\text{-}3b}$ or $I_{CLH\text{-}3b}$ measured in wild-type oocytes (9).

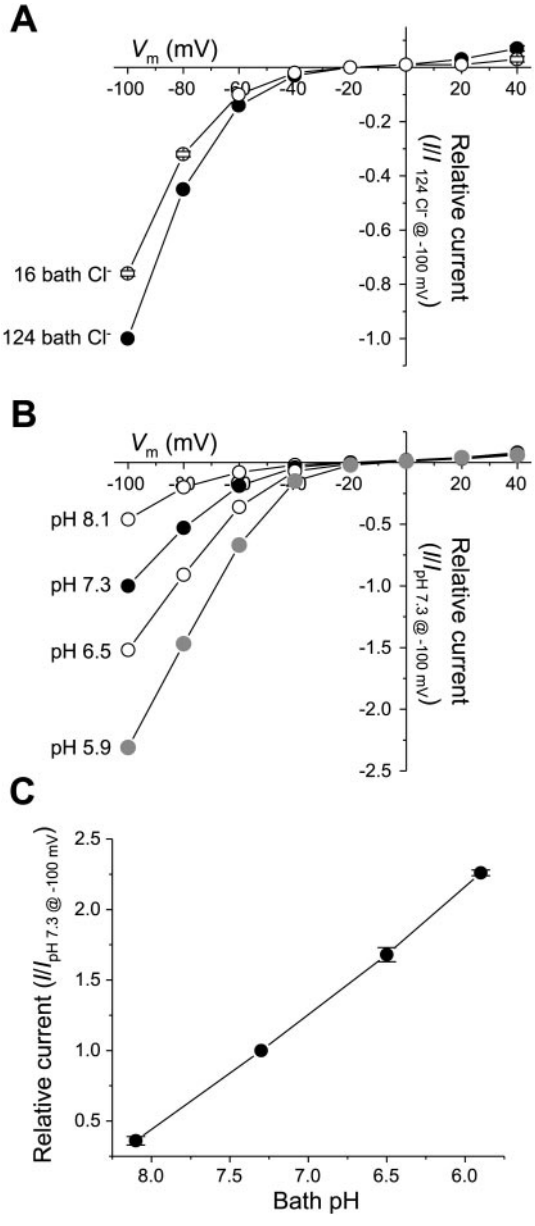

Fig. 6. Sensitivity of $I_{CLH\text{-}3b\Delta C}$ to reduction of extracellular Cl^- and pH. *A*: *I-V* relationships for $I_{CLH\text{-}3b\Delta C}$ recorded in 124 mM Cl^- control bath solution and 30 s after switching to a 16 mM Cl^- bath solution. Current values measured at each test potential were normalized to those measured at −100-mV in 124 mM Cl^- bath solution. Values are means ± SE ($n = 6$). *B*: representative *I-V* relationships for $I_{CLH\text{-}3b\Delta C}$ recorded in pH 7.3 control bath and 30 s after switching to pH 5.9, pH 6.5, or pH 8.1 bath solutions. *C*: effects of changes in extracellular pH on $I_{CLH\text{-}3b\Delta C}$ recorded at −100 mV. Values are means ± SE ($n = 5$).

Figure 6, *B* and *C*, shows the effect of changing bath pH on $I_{CLH\text{-}3b\Delta C}$. Reduction of bath pH from 8.1 to 5.9 increased steady-state $I_{CLH\text{-}3b\Delta C}$ amplitude ~6.3-fold at −100 mV. In contrast, a similar reduction of bath pH increases the amplitude of native and heterologously expressed $I_{CLH\text{-}3b}$ only approximately twofold (9).

Kinetics of inhibition by Zn^{2+} are altered in CLH-3bΔC. $I_{CLH\text{-}3b}$ in the *C. elegans* oocyte is inhibited by >90% by bath application of 10 mM Zn^{2+} (27). Because $I_{CLH\text{-}3b}$ and $I_{CLH\text{-}3b\Delta C}$ exhibit different sensitivities to extracellular Cl^- and pH, we tested whether they also differ in their sensitivity to extracellular Zn^{2+}. Oocytes were held at 0 mV and stepped to −100 mV every 2 s for 1 s during continuous perfusion of control bath or bath containing 5 mM Zn^{2+}. Figure 7, *A* and *C*, shows typical time course experiments for Zn^{2+}-induced inhibition of $I_{CLH\text{-}3b}$ and $I_{CLH\text{-}3b\Delta C}$, respectively. Zn^{2+} inhibited $I_{CLH\text{-}3b}$ with a biphasic time course that consisted of a rapid initial phase followed by a much slower secondary phase (Fig. 7*A*). The time course of Zn^{2+} inhibition of $I_{CLH\text{-}3b}$ could be fitted with a biexponential function describing τ_{fast} and τ_{slow} (Fig. 7*B*). Mean ± SE amplitudes of the fast (A_{fast}) and slow (A_{slow}) components were 0.69 ± 0.05 and 0.27 ± 0.04 ($n = 4$), respectively. In contrast, Zn^{2+} inhibited $I_{CLH\text{-}3b\Delta C}$ with a rapid monoexponential time course that lacked the slower phase observed during inhibition of $I_{CLH\text{-}3b}$ (compare Fig. 7, *A* and *C*). The time constant for Zn^{2+}-mediated inhibition of $I_{CLH\text{-}3b\Delta C}$ is shown in Fig. 7*D*. Mean ± SE amplitude was 0.90 ± 0.01 ($n = 7$). Mean ± SE inhibition of $I_{CLH\text{-}3b}$ and $I_{CLH\text{-}3b\Delta C}$ with 5 mM Zn^{2+} at −100 mV was 86 ± 2% ($n = 4$) and 90 ± 1% ($n = 7$), respectively. The extent of inhibition in the two channels was not significantly different ($P > 0.07$). Block of both $I_{CLH\text{-}3b}$ and $I_{CLH\text{-}3b\Delta C}$ was reversible, and Zn^{2+} washout followed similar monoexponential time courses that were not significantly different for the two channels ($P > 0.6$) (Fig. 7, *B* and *D*). Mean ± SE amplitudes of current recovery for $I_{CLH\text{-}3b}$ and $I_{CLH\text{-}3b\Delta C}$ were 0.11 ± 0.01 ($n = 4$) and 0.1 ± 0.03 ($n = 3$), respectively.

Predepolarization-induced potentiation of $I_{CLH\text{-}3b\Delta C}$ is blocked by Zn^{2+}. In addition to observing inhibition of total channel activity, we also found that Zn^{2+} blocked predepolarization-induced potentiation of $I_{CLH\text{-}3b\Delta C}$. Figure 8*A* shows mean current traces from three *clh-3*(*ok768*) oocytes recorded in control bath and in the presence of 100 μM Zn^{2+}, which blocks prepotentiation completely. A dose-response curve for Zn^{2+}-mediated inhibition of prepotentiation is shown in Fig. 8*B*. IC_{50} for Zn^{2+} inhibition of $I_{CLH\text{-}3b\Delta C}$ prepotentiation was 10 μM. Interestingly, Zn^{2+} concentrations up to 250 μM failed to block hyperpolarization-activated $I_{CLH\text{-}3b\Delta C}$. Mean ± SE steady-state $I_{CLH\text{-}3b\Delta C}$ amplitudes recorded at −100 mV in control saline and in the presence of 250 μM Zn^{2+} were −21 ± 8 pA/pF and −21 ± 9 pA/pF ($n = 3$), respectively. These values were not significantly different ($P > 0.9$).

DISCUSSION

We showed previously that heterologous expression of CLH-3a and CLH-3b gives rise to currents with distinct functional properties (9). Several characteristics of $I_{CLH\text{-}3a}$ and

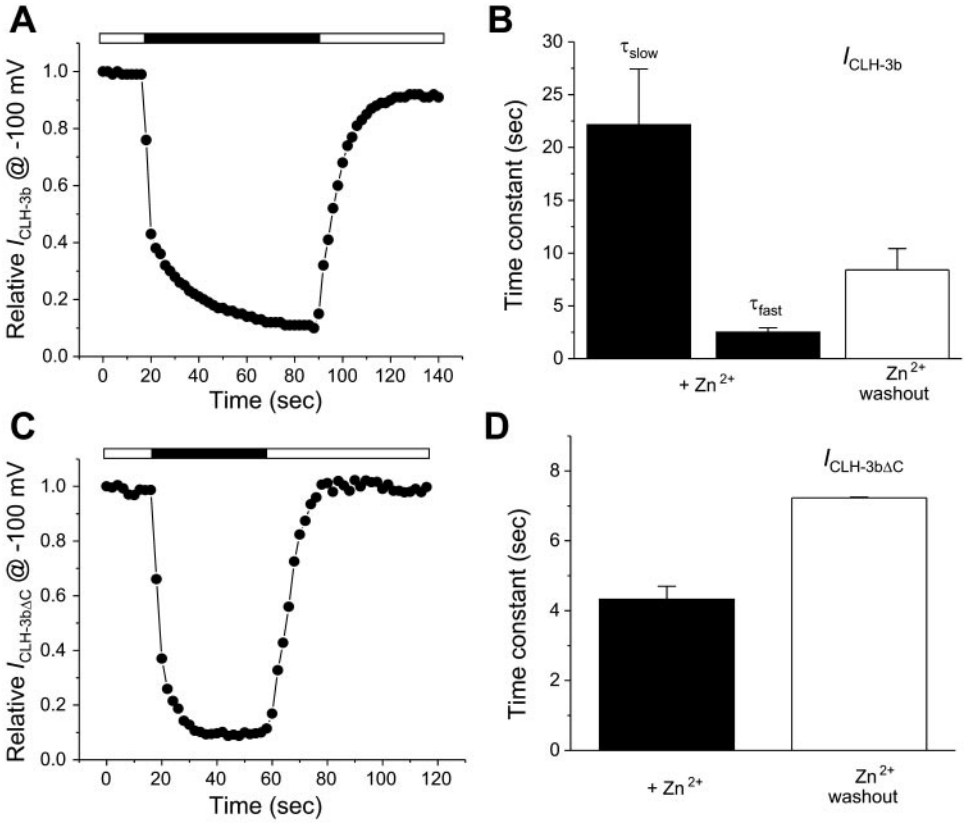

Fig. 7. Kinetics of Zn^{2+}-mediated inhibition of I_{CLH-3b} and $I_{CLH-3b\Delta C}$. *A*: representative time course of Zn^{2+}-induced inhibition of I_{CLH-3b}. I_{CLH-3b} was activated by excluding ATP from the pipette solution. Current amplitude was recorded by repetitively stepping to −100 mV every 2 s from a holding potential of 0 mV during continuous perfusion with control solution (open bar) and 5 mM Zn^{2+}-containing bath solution (solid bar). *B*: time constants for Zn^{2+}-mediated inhibition of I_{CLH-3b} ($+Zn^{2+}$) and reversal during Zn^{2+} washout. Inhibition of I_{CLH-3b} by Zn^{2+} was fit by a biexponential function yielding fast-activation time constants (τ_{fast}) and slow-activation time constants (τ_{slow}), whereas washout of Zn^{2+} followed a single exponential time course. Values are means ± SE (n = 4). *C*: representative time course of Zn^{2+}-mediated inhibition of $I_{CLH-3b\Delta C}$. $I_{CLH-3b\Delta C}$ amplitude was measured as described for I_{CLH-3b} during continuous perfusion with control or 5 mM Zn^{2+}-containing bath solution. *D*: time constants of Zn^{2+}-mediated inhibition of $I_{CLH-3b\Delta C}$ ($+Zn^{2+}$) and reversal during Zn^{2+} washout. The time courses of inhibition of $I_{CLH-3b\Delta C}$ by Zn^{2+} and washout were fitted with single exponential functions. Values are means ± SE (n = 3–7).

I_{CLH-3b} observed in human embryonic kidney HEK cells and I_{CLH-3b} and $I_{CLH-3b\Delta C}$ recorded in the worm oocyte are summarized in Table 1. The voltage sensitivity of CLH-3a is reduced, and its activation kinetics are slower than those of CLH-3b. Unlike CLH-3a, CLH-3b exhibits no depolarization-induced potentiation behavior and exhibits greatly reduced sensitivity to extracellular pH and Cl^- concentration (Table 1).

The major sequence differences in the two splice variants include a 71-amino acid NH_2-terminal extension on CLH-3a and 270 additional amino acids in the CLH-3b COOH terminus (Fig. 1*C*). Elongation of the CLH-3b COOH terminus includes a 101-amino acid domain inserted between CBS1 and CBS2 and a 169-amino acid COOH-terminal extension (Fig. 1*C*). A simple hypothesis to explain the functional differences of the channels is that the unique NH_2 terminus of CLH-3a gives rise to its increased pH and Cl^- sensitivity as well as to its sensitivity to depolarization. Alternatively, the COOH terminus of CLH-3b may suppress sensitivity to depolarization and extracellular ions.

As shown in Table 1, the characteristics of $I_{CLH-3b\Delta C}$ suggest that the COOH terminus plays an important role in controlling channel properties. The *clh-3*(*ok768*) allele is a 165-amino acid COOH-terminal deletion that encompasses the 101-amino acid insert between the CLH-3b CBS domains and another 64-amino acids upstream of this region that are shared by both variants (Fig. 1*C*). Deletion of this region increases channel pH and Cl^- sensitivity (Fig. 6), reduces sensitivity to hyperpolarizing voltages and slows hyperpolarization-induced activation kinetics (Fig. 4), and induces depolarization-induced prepotentiation behavior (Fig. 5).

The properties of CLH-3bΔC resemble but do not fully recapitulate those of heterologously expressed CLH-3a. It is noteworthy that the stimulatory effects of bath acidification, elevated bath Cl^-, and a 3-s predepolarization to 60 mV on CLH-3a are about twice those observed for CLH-3bΔC (Table 1). This suggests that the CLH-3a NH_2 terminus may be required for full sensitivity to these parameters or that sensitivity to depolarization and extracellular ions is also modulated by the 169-amino acid extension of the CLH-3b COOH terminus. Site-directed mutagenesis and heterologous expression studies are required to fully define the role of NH_2 and COOH termini in CLH-3 channel gating.

Bacterial ClC crystal structures (12, 13) have demonstrated that the last α-helix, or R helix, immediately preceding the cytoplasmic COOH terminus contributes a tyrosine residue that protrudes into the channel pore and functions in Cl^- coordination. Amino acid residues thought to be involved in ClC fast gating and pore Cl^- binding (12, 13) are fully conserved in CLH-3a and CLH-3b. We suggested previously (9) that the differences in extracellular H^+ and Cl^- sensitivity of the splice variants (see Table 1) might be due to structural changes in the CLH-3b COOH terminus that secondarily alter the structure of the R helix and the accessibility and/or function of pore-associated ion-binding sites. Recent studies by Hebeisen and Fahlke (17) are consistent with this idea and have shown clearly that truncation of the COOH terminus alters the conformation of the outer vestibule of ClC-1.

We also suggested previously (9) that the effect of depolarization on channel activation could be due to effects of changes in local Cl^- concentration on a fast gating mechanism. How-

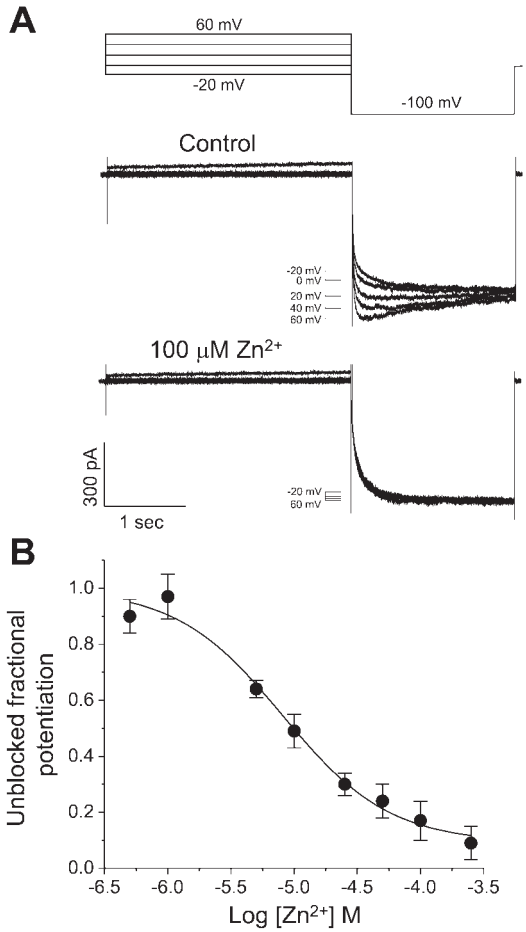

Fig. 8. Inhibition of predepolarization-induced potentiation of $I_{CLH\text{-}3b\Delta C}$ by Zn^{2+}. *A*: effect of conditioning potential on hyperpolarization-induced activation of $I_{CLH\text{-}3b\Delta C}$ in the absence and presence of 100 μM Zn^{2+}. The voltage-clamp protocol used was the same as that described in Fig. 5. *B*: dose-response relationship of Zn^{2+}-mediated inhibition of predepolarization-induced potentiation of $I_{CLH\text{-}3b\Delta C}$ amplitude after 60-mV CP relative to that after −20-mV CP. Dose-response relationship was fit using a Boltzmann function to determine IC_{50}. Values are means ± SE (n = 3–7).

ever, the data shown in Fig. 8 suggest that depolarization-induced potentiation may be mediated at least in part by a slow gating process. Extracellular Cd^{2+} and Zn^{2+} inhibit ClC channels (7, 11, 21, 31), including CLH-3b (27) (Fig. 7*A*). Studies of ClC-0 (7) and ClC-2 (31) have suggested that facilitation of slow gating is responsible for the inhibitory effects of these cations. In ClC-1, Zn^{2+} inhibition is thought to be mediated by binding of the ion to a closed state of the slow gate (11). It is conceivable that depolarization-induced opening of the CLH-3bΔC slow gate is responsible for potentiation. Interestingly, we found that micromolar concentrations of extracellular Zn^{2+} inhibit depolarization-induced potentiation with an IC_{50} of 10 μM (Fig. 8) but have no effect on hyperpolarization-induced current amplitude. If potentiation involves a slow gating mechanism, micromolar levels of Zn^{2+} may disrupt depolarization-induced conformational changes that are required for opening of the gate. Detailed analysis of CLH-3 single-channel properties is needed to fully assess how voltage, extracellular ions, and NH_2-terminal and COOH-terminal splice variations modulate fast and slow gating processes.

Exposure to 5 mM Zn^{2+} caused a rapid and reversible ~90% inhibition of both CLH-3b and CLH-3bΔC (Fig. 7). However, the kinetics of Zn^{2+} inhibition for the two channels are considerably different. Fast and slow processes mediate Zn^{2+} inhibition of CLH-3b (Fig. 7, *A* and *B*), whereas inhibition of CLH-3bΔC occurs by a rapid process that can be described by a single exponential (Fig. 7, *C* and *D*). Divalent cation inhibition of ClC-0, ClC-1, and ClC-2 is thought to be mediated in part by Zn^{2+} binding to specific extracellular cysteine residues. In ClC-1, for example, three cysteine residues that participate in Zn^{2+}-dependent channel inhibition have been identified on the basis of site-directed mutagenesis studies (21). The altered Zn^{2+} inhibition of CLH-3bΔC suggests that changes in the structure of the intracellular COOH terminus may modulate the accessibility and Zn^{2+}-binding kinetics of cysteine and/or other amino acid residues on the extracellular face of the channel.

CLH-3b is activated by oocyte swelling and meiotic cell cycle progression (27). Activation is mediated by serine/threonine dephosphorylation events (10, 28). Deletion mutation of the CLH-3b COOH terminus dramatically alters channel regulation. CLH-3bΔC is insensitive to oocyte shrinkage (see RESULTS) and ATP depletion (Fig. 3*B*). These experimental maneuvers respectively inhibit (27) and dramatically activate CLH-3b (28). In addition, CLH-3b is activated >20-fold by oocyte swelling, whereas CLH-3bΔC is activated only ~1.2-fold (Fig. 3*A*). Loss of CLH-3bΔC volume sensitivity and activation by ATP depletion suggests that the deleted amino acids are involved in channel regulation. The deleted region contains several potential phosphorylation sites, a binding site for germinal center kinase-3, or GCK-3, which is a new member of the sterile 20 (Ste20) serine/threonine kinase superfamily that functions to inhibit CLH-3b (10), and a highly charged region that could mediate regulatory protein-protein

Table 1. *Comparison of the effects of depolarization and bath pH and Cl^- concentration on HEK cells expressing CLH-3a and CLH-3b and on CLH-3b and CLH-3bΔC expressed in the C. elegans oocyte*

	Potentiation by +60-mV CP*	Inactivation After +60-mV CP*	Activation by pH 5.9 Bath†	Inhibition by Low Bath Cl^-
HEK CLH-3a	2-fold	20%	12-fold	40%
HEK CLH-3b	None	None	2-fold	None
C. elegans oocyte CLH-3b	None	None	2-fold	None
C. elegans oocyte CLH-3bΔC	1.5-fold	15%	6-fold	24%

Data on human embryonic kidney (HEK) cells expressing CLH-3a and CLH-3b and on *Caenorhabditis elegans* oocyte CLH-3b are summarized from Denton et al. (9). All currents were recorded at −100 mV. Identical voltage-clamp protocols and changes in bath Cl^- levels and pH were used in HEK cell and *C. elegans* oocyte experiments. *Values are relative to a conditioning potential (CP) of −20 mV. †Values are relative to those measured at a bath pH of 8.1.

interactions and/or regulatory interactions within the channel protein itself.

In conclusion, we have characterized a CLH-3b COOH-terminal deletion mutant in its native cellular environment, where regulatory interactions with other proteins are presumably minimally perturbed. Our results demonstrate clearly that the cytoplasmic COOH terminus plays important roles in channel gating and regulation. Site-directed mutagenesis studies are clearly warranted to begin defining the underlying structural and functional relationships of the COOH terminus. Our findings contribute to a growing body of evidence indicating that NH_2- and COOH-terminal cytoplasmic domains are essential for the function of eukaryotic ClCs and likely contribute significantly to the evolution and physiological diversification of these channels.

ACKNOWLEDGMENTS

The *clh-3*(*ok768*) worms were provided by the *C. elegans* Gene Knockout Project at Oklahoma Medical Research Foundation, which is part of the International *C. elegans* Gene Knockout Consortium (http://www.mutantfactory.ouhsc.edu/).

GRANTS

This work was supported by National Institute of Diabetes and Digestive and Kidney Diseases (NIDDK) Grants R01 DK-51618 and P01 DK-58212 (to K. Strange), National Institute of General Medical Sciences National Research Service Award F32 GM-067424.01 (to J. Denton), and NIDDK Grant R21 DK-062763 (to K. Nehrke).

REFERENCES

1. **Accardi A and Pusch M.** Conformational changes in the pore of CLC-0. *J Gen Physiol* 122: 277–293, 2003.
2. **Bargmann CI.** Neurobiology of the *Caenorhabditis elegans* genome. *Science* 282: 2028–2033, 1998.
3. **Bateman A.** The structure of a domain common to archaebacteria and the homocystinuria disease protein. *Trends Biochem Sci* 22: 12–13, 1997.
4. **Beck CL, Fahlke C, and George AL Jr.** Molecular basis for decreased muscle chloride conductance in the myotonic goat. *Proc Natl Acad Sci USA* 93: 11248–11252, 1996.
5. **Bennetts B, Roberts ML, Bretag AH, and Rychkov GY.** Temperature dependence of human muscle ClC-1 chloride channel. *J Physiol* 535: 83–93, 2001.
6. **Brenner S.** The genetics of *Caenorhabditis elegans*. *Genetics* 77: 71–94, 1974.
7. **Chen TY.** Extracellular zinc ion inhibits ClC-0 chloride channels by facilitating slow gating. *J Gen Physiol* 112: 715–726, 1998.
8. **Cid LP, Niemeyer MI, Ramírez A, and Sepúlveda FV.** Splice variants of a ClC-2 chloride channel with differing functional characteristics. *Am J Physiol Cell Physiol* 279: C1198–C1210, 2000.
9. **Denton J, Nehrke K, Rutledge E, Morrison R, and Strange K.** Alternative splicing of N- and C-termini of a *C. elegans* ClC channel alters gating and sensitivity to external Cl^- and H^+. *J Physiol* 555: 97–114, 2004.
10. **Denton J, Nehrke K, Yin X, Morrison R, and Strange K.** GCK-3, a newly identified Ste20 kinase, binds to and regulates the activity of a cell cycle-dependent ClC anion channel. *J Gen Physiol* 125: 113–125, 2005.
11. **Duffield MD, Rychkov GY, Bretag AH, and Roberts ML.** Zinc inhibits human ClC-1 muscle chloride channel by interacting with its common gating mechanism. *J Physiol* 568: 5–12, 2005.
12. **Dutzler R, Campbell EB, Cadene M, Chait BT, and MacKinnon R.** X-ray structure of a ClC chloride channel at 3.0 Å reveals the molecular basis of anion selectivity. *Nature* 415: 287–294, 2002.
13. **Dutzler R, Campbell EB, and MacKinnon R.** Gating the selectivity filter in ClC chloride channels. *Science* 300: 108–112, 2003.
14. **Estévez R, Pusch M, Ferrer-Costa C, Orozco M, and Jentsch TJ.** Functional and structural conservation of CBS domains from CLC chloride channels. *J Physiol* 557: 363–378, 2004.
15. **Fong P, Rehfeldt A, and Jentsch TJ.** Determinants of slow gating in ClC-0, the voltage-gated chloride channel of *Torpedo marmorata*. *Am J Physiol Cell Physiol* 274: C966–C973, 1998.
16. **Gründer S, Thiemann A, Pusch M, and Jentsch TJ.** Regions involved in the opening of ClC-2 chloride channel by voltage and cell volume. *Nature* 360: 759–762, 1992.
17. **Hanke W and Miller C.** Single chloride channels from *Torpedo* electroplax: activation by protons. *J Gen Physiol* 82: 25–45, 1983.
18. **Haug K, Warnstedt M, Alekov AK, Sander T, Ramírez A, Poser B, Maljevic S, Hebeisen S, Kubisch C, Rebstock J, Horvath S, Hallmann K, Dullinger JS, Rau B, Haverkamp F, Beyenburg S, Schulz H, Janz D, Giese B, Müller-Newen G, Propping P, Elger CE, Fahlke C, Lerche H, and Heils A.** Mutations in *CLCN2* encoding a voltage-gated chloride channel are associated with idiopathic generalized epilepsies. *Nat Genet* 33: 527–532, 2003.
19. **Hebeisen S and Fahlke C.** Carboxy-terminal truncations modify the outer pore vestibule of muscle chloride channels. *Biophys J* 89: 1710–1720, 2005.
20. **Jentsch TJ, Stein V, Weinreich F, and Zdebik AA.** Molecular structure and physiological function of chloride channels. *Physiol Rev* 82: 503–568, 2002.
21. **Kürz LL, Klink H, Jakob I, Kuchenbecker M, Benz S, Lehmann-Horn F, and Rüdel R.** Identification of three cysteines as targets for the Zn^{2+} blockade of the human skeletal muscle chloride channel. *J Biol Chem* 274: 11687–11692, 1999.
22. **Miller C and White MM.** Dimeric structure of single chloride channels from *Torpedo* electroplax. *Proc Natl Acad Sci USA* 81: 2772–2775, 1984.
23. **Nehrke K, Begenisich T, Pilato J, and Melvin JE.** Model organisms: new insights into ion channel and transporter function. *Caenorhabditis elegans* ClC-type chloride channels: novel variants and functional expression. *Am J Physiol Cell Physiol* 279: C2052–C2066, 2000.
24. **Plasterk RH.** Reverse genetics: from gene sequence to mutant worm. *Methods Cell Biol* 48: 59–80, 1995.
25. **Pusch M.** Myotonia caused by mutations in the muscle chloride channel gene *CLCN1*. *Hum Mutat* 19: 423–434, 2002.
26. **Pusch M, Ludewig U, and Jentsch TJ.** Temperature dependence of fast and slow gating relaxations of ClC-0 chloride channels. *J Gen Physiol* 109: 105–116, 1997.
27. **Rutledge E, Bianchi L, Christensen M, Boehmer C, Morrison R, Broslat A, Beld AM, George AL Jr, Greenstein D, and Strange K.** CLH-3, a ClC-2 anion channel ortholog activated during meiotic maturation in *C. elegans* oocytes. *Curr Biol* 11: 161–170, 2001.
28. **Rutledge E, Denton J, and Strange K.** Cell cycle- and swelling-induced activation of a *C. elegans* ClC channel is mediated by CeGLC-7α/β phosphatases. *J Cell Biol* 158: 435–444, 2002.
29. **Schriever AM, Friedrich T, Pusch M, and Jentsch TJ.** CLC chloride channels in *Caenorhabditis elegans*. *J Biol Chem* 274: 34238–34244, 1999.
30. **Shimada K, Li X, Xu G, Nowak DE, Showalter LA, and Weinman SA.** Expression and canalicular localization of two isoforms of the ClC-3 chloride channel from rat hepatocytes. *Am J Physiol Gastrointest Liver Physiol* 279: G268–G276, 2000.
31. **Zuñiga L, Niemeyer MI, Varela D, Catalán M, Cid LP, and Sepúlveda FV.** The voltage-dependent ClC-2 chloride channel has a dual gating mechanism. *J Physiol* 555: 671–682, 2004.